Design and Performance Validation of a Compact Wireless Ultrasonic Device for Localized Damage Detection

Shuo Chen[1, 2], Xinjun Dong[2], Jin-Yeon Kim[2], Shengxing Wu[1], Yang Wang[2,*]

[1]*College of Civil and Transportation Engineering, Hohai University, Nanjing, 210098, China*

[2]*School of Civil and Environmental Engineering, Georgia Institute of Technology, Atlanta, GA 30332, USA*

Abstract: Recent years have seen growing adoption of wireless structural sensor nodes that can significantly reduce the cost and installation effort of a structural health monitoring system. While previous wireless sensor development has mainly focused upon dynamic and vibration measurements at lower frequency domains, in this study, a new wireless ultrasonic sensing node capable of megahertz excitation and sampling is proposed. In addition to presenting the design of the wireless ultrasonic sensing node, experimental notch test and fatigue test of a dog-bone specimen are described in this paper. The experimental results demonstrate that the ultrasonic characteristics of surface cracks can be identified in both scenarios with the proposed wireless sensor node. Furthermore, a signal processing procedure is proposed to obtain an accurate estimation of the ultrasonic signal amplitude, which can be a key indicator for crack identification. The procedure involves signal reconstruction with the cardinal sine function and envelope detection using discrete Hilbert transform.

Keywords: fatigue crack, Hilbert transform, notch test, structural health monitoring, ultrasonic measurement, wireless sensing

1. Introduction

Throughout the decades of its service life, a civil structure can experience various adverse environmental conditions (e.g. extreme weather condition, frost-wedging, and freeze-thaw cycles) and excessive loads (e.g. overloaded trucks), both of which may gradually lead to structural deterioration. Infrastructure deterioration has become an issue of concern in both developed and developing countries. According to the ASCE 2013 Report Card for America's Infrastructure, 1/9 of the nation's bridges are classified as structurally deficient. Meanwhile, 32% of America's major roads are in poor or mediocre condition, which costs U.S. motorists $67 billion a year in repairs and operation. With limited maintenance budget for repair, it is important to be aware of updated structural conditions in real time, in order to determine which structures are in the direst situation.

To collect real-time information on infrastructure conditions, a vast amount of structural health monitoring (SHM) techniques have been studied. Overall, the approaches can be classified as either passive or active. Passive SHM methods collect sensor signals from the structure without generating excitation signals first (Dhakal, et al. 2013). Acoustic emission technique, for instance, is a typical passive SHM method used to detect elastic waves generated in a continuous cracking process (Ohtsu 1996). In contrast,

[*]Corresponding author, Email address: yang.wang@ce.gatech.edu; Tel: +1 (404) 894-1851.

active SHM is different by generating excitation signals to intentionally excite the structure and then measure the response. Therefore, the active SHM methods can be more controllable compared with the passive ones. Ultrasound technique is a widely used active SHM method, which employs a transducer to generate excitation signals and detect structural response. The response signal may indicate the presence, extent, intensity and geometric shape of the damage (Grosse, et al. 2004). Different types of ultrasonic waves can be used for SHM, such as Rayleigh wave, longitudinal wave and shear wave (Aindow, et al. 1981). Main advantages of the Rayleigh wave include: (1) the wave propagation suffers less from geometric attenuation than three dimensional waves (Pertsch 2009), (2) Rayleigh wave is non-dispersive (Viktorov 1967), and (3) Rayleigh wave is naturally sensitive to surface or near-surface defects or material degradation. For these reasons, Rayleigh wave is best suited for measuring the surface crack depth with a low-power ultrasonic SHM device (such as the one described in this paper). However, one should be aware that a major disadvantage is that Rayleigh wave loses its sensitivity when a crack is deeper than a few times of the wavelength.

Although cabled ultrasonic SHM technologies are relatively mature, the technologies are generally more suitable for short-term inspection rather than long-term monitoring in the field. Commercial ultrasonic equipment is bulky and too expensive to be left for long-term field operations (Monje, et al. 2012). For locations difficult to reach, it is even more unfeasible to carry ultrasonic equipment for in-situ test, due to the weight and size of the equipment. In order to reduce the cost and improve the equipment portability, SHM systems adopting wireless communication technology have been investigated. An exhaustive review on wireless sensing for SHM is provided by Lynch and Loh (2006), which summarizes the development of various academic and industrial wireless sensing devices. Many field experiments have been performed to validate the performance of wireless sensing devices. For instance, a field test is carried out on the Geumdang Bridge located in Incheon, Korea by Lynch, *et al.* (2006), and the result shows that the wireless sensor data has comparable quality with cabled data. With growing interest and development in wireless sensor network, many other research teams have also made significant development (Baker, et al. 2011; Warneke and Pister 2004). Wireless sensor devices are becoming more energy efficient and the cost has been continuously reducing (Nakamura, et al. 2013).

To combine the advantages of traditional SHM and NDE systems, a preliminary prototype device for wireless ultrasonic evaluation has been developed by Pertsch, *et al.* (2011). This device is smaller in size compared with traditional NDE systems, but still consists of multiple separate physical components that are somewhat cumbersome. These components include an evaluation board for the Texas Instruments F28335 microprocessor, a connector board for wireless transceiver, an excitation signal amplification board, and a receiving signal conditioning board. The device is tested on a specimen with artificial notches cut by electrical discharge machining, but no fatigue crack test is reported.

In comparison, the wireless ultrasonic device developed in this study demonstrates significant improvement in hardware integration. The development in this study is based upon a latest generation of wireless sensing platform, named *Martlet* (Kane, et al. 2014). The highly integrated *Martlet* motherboard ($6.35\text{cm} \times 5.71\text{cm}$) contains a microprocessor and a wireless transceiver onboard. The ultrasonic board developed in this study, which has similar size to the motherboard, easily stacks on top of the motherboard (Dong, et al. 2014) and achieves a significantly more compact configuration than the previous prototype. In addition, a two-step data processing is proposed in this study, including signal reconstruction and then envelope extraction. Finally, a fatigue crack test is conducted with the newly developed wireless ultrasonic device for more realistic performance validation.

This paper presents the design and validation of the wireless ultrasonic sensing node aimed to provide the advantages of being cable-free, low-cost, and miniaturized, yet still being functionally comparable with traditional cable-based ultrasonic equipment. Section 2 describes the hardware design of the ultrasonic device. In Section 3, a two-step algorithm (i.e. signal reconstruction and envelope detection) is proposed to obtain close approximation of a received ultrasonic signal. Using a notch specimen, Section 4 illustrates the measurement comparison of the wireless ultrasonic device and commercial cabled equipment. Section 5 describes measurement results in a laboratory fatigue experiment with a dog-bone specimen. Section 6 provides a summary of the work.

2. General concept and hardware architecture

The wireless ultrasonic sensing node proposed in this study is developed upon the *Martlet* wireless sensing platform (Kane, et al. 2014). Featuring a Texas Instruments Piccolo microcontroller as the core

processor, *Martlet* is a low-cost wireless sensing platform for various structural health-monitoring applications. The clock frequency of an earlier version (TMX320F28069) of the microcontroller can be programmed up to 80 MHz, and a more recent version (TMS320F28069) can support up to 90 MHz. Using the earlier version of microcontroller, the onboard analog-to-digital conversion (ADC) module can sample data at a frequency up to 2.67 MHz. While using the more recent microcontroller version, the sampling rate can achieve 3 MHz. The *Martlet* node adopts a 2.4 GHz radio for low-power wireless communication through IEEE 802.15.4 standard (Cooklev 2004). The communication range can reach up to 500m at line-of-sight, and the maximum transfer rate can reach 250 kbps.

The extensible hardware design feature of the *Martlet* motherboard enables various accessory sensor boards to conveniently stack up through four wing connectors and work with the *Martlet* motherboard. The combination of the extensible design feature with onboard 9-channel 12-bit ADC allows the *Martlet* node to simultaneously sample analog signals from multiple sensors through different accessory sensor boards (termed "wing" boards). This study primarily utilizes the newly developed ultrasonic wing (as shown in Figure 1) for ultrasonic excitation and receiving, following a pitch-catch setup of ultrasonic transducers.

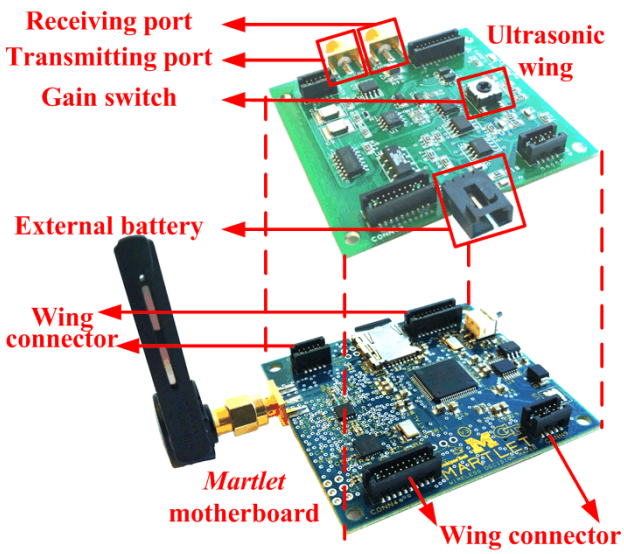

Figure 1. Schematic diagram of the ultrasonic wing stacking on the *Martlet* motherboard

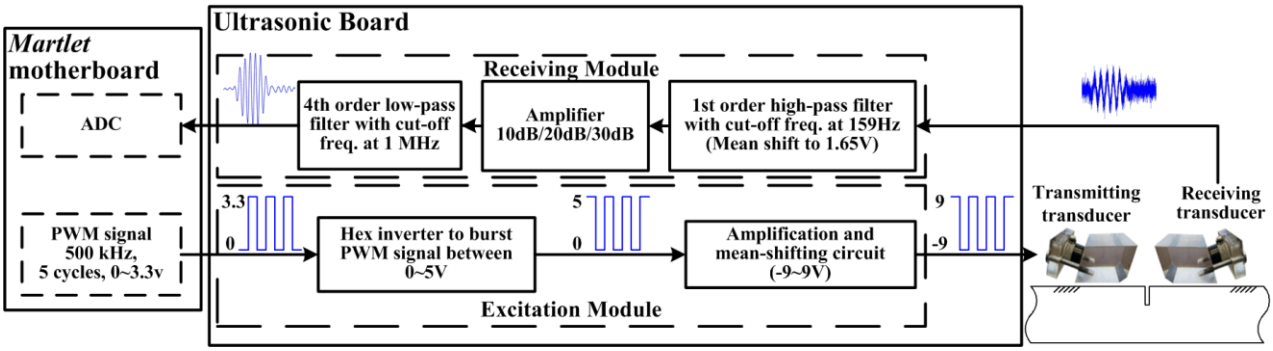

Figure 2. Functional diagram of the ultrasonic wing developed for the *Martlet* wireless sensing node; the ultrasonic wing contains an excitation module and a receiving module

Figure 2 shows the functional diagram of the ultrasonic wing, which constitutes of two modules, an excitation module and a receiving module. The excitation module amplifies 5-cycle bursts of 500 kHz pulse-width modulation (PWM) signals, which are originally generated by *Martlet* by certain amplification gain. When powered by two standard low-cost 9-volt batteries, the output of the excitation module occupies the voltage range of -9 V to +9 V. Although ±9 V range is used this study, when higher-voltage power source is available, e.g. by simply connecting two 9-volt batteries in series, the range can be easily increased till up to ±20 V when needed. The burst signals are then fed into the transmitting transducer to generate ultrasonic waves as the excitation source for the transmitting transducer. The transmitting transducer then launches ultrasonic waves along a solid structural surface. Upon propagation, a receiving transducer catches the response signal, which is then collected by the receiving module of the ultrasonic wing. Signal conditioning circuit in the receiving module shifts, filters and amplifies the response signals captured by the receiving transducer, and then transfers the analog signal to the ADC module of the microcontroller in *Martlet* motherboard.

2.1. Excitation signal generation

The generation of ultrasonic excitation signal is first initiated by the PWM module of the microcontroller in *Martlet* motherboard, and then amplified and shifted by the excitation module of the ultrasonic wing. The PWM module can generate square waves between 0~3.3 V at 500 kHz, which meets the center frequency of the commercial ultrasonic transducers adopted for this study (*Ultran Group* WC50-0.5). The signal amplification module in the ultrasonic wing aims to boost the PWM signal to a higher level. When two pieces of standard 9 V batteries are used, one providing +9 V and the other providing -9V, the schematic is shown in Figure 3. Because of the high-speed switching of the PWM signal, a MOSFET

(*Alpha & Omega Semiconductor Inc.* AO4612) amplifier circuit is used to buffer the 0~3.3 V signal generated by the PWM module of the *Martlet* motherboard. Because the amplitude of the signal initiated by *Martlet* is only 3.3 V and does not meet the threshold voltage requirement between the MOSFET gate (G) and source (S), a hex inverter (*Texas Instruments* 74LS04) is adopted to boost the PWM signals to 0~5 V. The amplification circuit consists of two halves. The positive half buffers the signal from 3.3 V to 9 V with a p-channel MOSFET, and the negative half changes the signal from 3.3 V to -9 V by an n-channel MOSFET. As a result, the signal is amplified by both positive and negative halves, and the output is fed into the transmitting ultrasonic transducer.

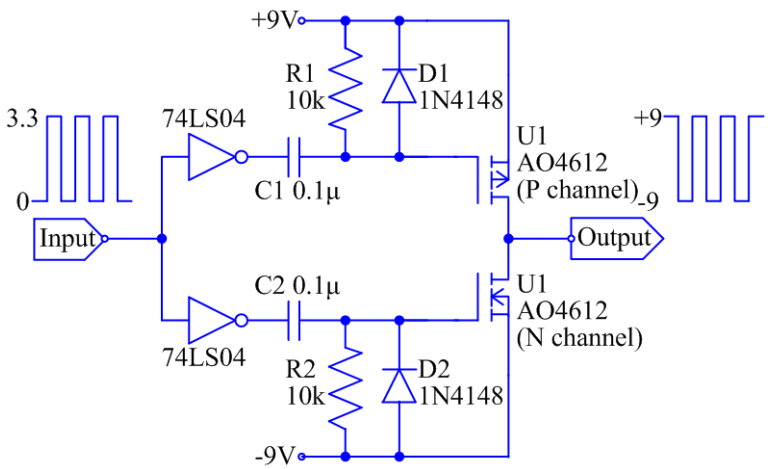

Figure 3. Schematic of the amplification circuit in the excitation module of the *Martlet* ultrasonic wing

2.2. Signal conditioning in the receiving module

Upon propagation of the ultrasonic waves along a solid surface, the signal captured by the receiving transducer has relatively low amplitude. A typical output of a received signal coming out of the receiving ultrasonic transducer oscillates between -0.02 V and +0.02 V. This signal cannot be fed into the *Martlet* ADC (analog-to-digital conversion) module directly, as the ADC module requires an input voltage between 0 V and 3.3 V. Therefore, the signal captured by the receiving transducer needs to be shifted, amplified, and filtered before entering the ADC module. Figure 4 shows the circuit schematic of the receiving module of the *Martlet* ultrasonic wing. The incoming signal, which oscillates around 0 V and contains negative voltages, first goes through a high-pass filter with a virtual ground at +1.65 V, so that the mean value of the signal is shifted up from 0 V to +1.65 V. The high-pass filter has a cutoff frequency set at 1.59 kHz, which

removes the low-frequency component in the signal, but is not high enough to affect the ultrasonic signal that has a center frequency at 500 kHz. The shifted signal then goes into a non-inverting amplifier with an adjustable gain. The gain can be easily switched among 10 dB, 20 dB and 30 dB. The last stage of the signal conditioning in the receiving module is a 4th-order Voltage Controlled Voltage Source (VCVS) low-pass Bessel filter. The low-pass cutoff frequency is set at 1 MHz. The filter offers a linear phase performance, which helps maintain the signal waveform in the time domain (Zhu, et al. 2011). This is important for identifying the arrival time of the received signal, which is an important index for ultrasonic data interpretation. Finally, the signal enters the *Martlet* ADC module and is transmitted back wirelessly after digitization.

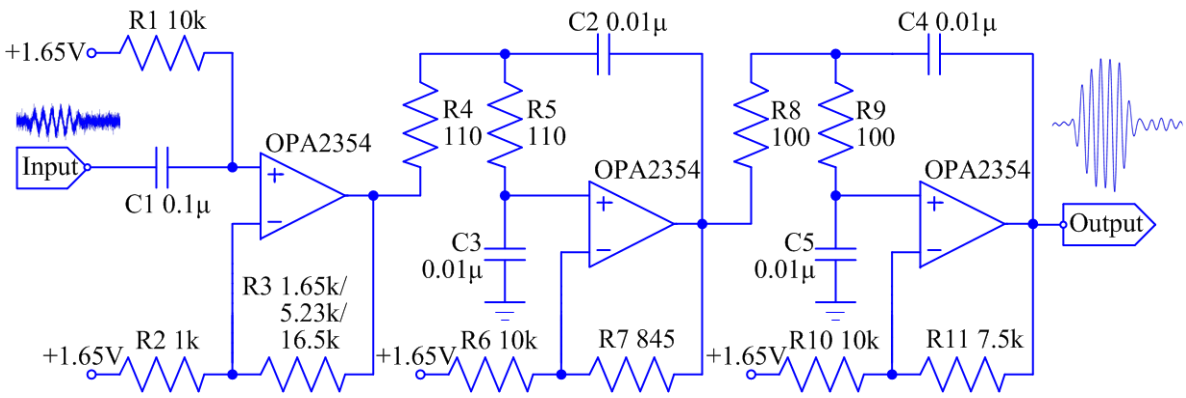

Figure 4. Schematic of the signal-conditioning circuit in the receiving module of the *Martlet* ultrasonic wing

3. Data processing

3.1. Signal reconstruction with the cardinal sine (sinc) function

The commercial ultrasonic transducers adopted in this study are the *Ultran Group* WC50-0.5 model with 500 kHz central frequency, which means that the received signal is mainly concentrated around 500 kHz, with a side lobe bandwidth usually less than 200 kHz. Therefore, according to the Nyquist-Shannon sampling theorem (Nyquist 1928; Shannon 1949), the sampling frequency used in this study (2 MHz) is sufficient for capturing the received signal. However, it is still possible that the digitization process cannot capture the exact peak of every received burst response, while the peak amplitude can be important for quantitative damage assessment. In order to obtain accurate waveform of the received signals, signal reconstruction for up-sampling is proposed as the first step of the two-step data processing.

In this study, the cardinal sine function (aka. sinc function) is adopted for signal reconstruction (Shannon 1948). The function enables reconstruction of band-limited signals (Yaroslavsky 2007). The formulation of the reconstructed signal reconstruction, $x_{re}(t)$, is as follows.

$$x_{re}(t) = \sum_{i=1}^{n} x[i] \cdot \mathrm{sinc}\left(t \cdot f_s - (i-1)\right) \tag{1}$$

where t represents time, f_s is the sampling frequency of the original signal (2 MHz in this study), $x[i]$ is the ith discrete sample point of the original signal, n is the number of data points, and $\mathrm{sinc}(x) = \sin(\pi x)/(\pi x)$.

3.2. *Envelope detection using Discrete Hilbert Transform*

In this paper, envelope amplitude is adopted as the indicator for quantitative damage assessment. It is important to calculate amplitude value as accurately as possible. However, if a simple peak-picking process is adopted, the original peak can be easily missed during the modulation process for transmission. Figure 5 shows an example for illustration. Signal 1 (dashed line) is a modulated signal, which happens to capture the original peak. Meanwhile, signal 2 (dot line) shows a more common scenario with original peak missed, but shares the same envelope with signal 1. Therefore, a more accurate estimation of the amplitude can be obtained from the envelope of the signal, compared with simple peak-picking. Discrete Hilbert transform (DHT) is adopted in this paper to detect the envelope. Proposed by Huang *et al*. (1998), Hilbert transform has been widely used as an analysis and processing method for nonlinear and non-stationary signals. Using the Cauchy principal value (CPV), Hilbert transform of the reconstructed signal is defined as:

$$\overline{x_{re}(t)} = \mathcal{H}\left\{x_{re}(t)\right\} = \frac{1}{\pi}\mathrm{CPV}\int_{-\infty}^{+\infty} \frac{x_{re}(\tau)}{t-\tau} d\tau \tag{2}$$

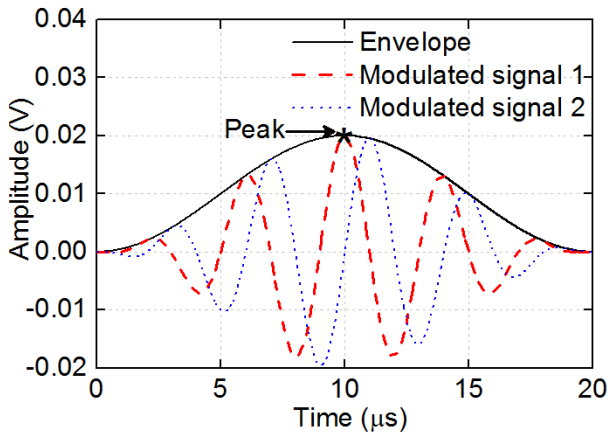

Figure 5. Diagram for two modulated signals sharing a same envelope waveform

Based on the definition, it can be seen that $\overline{x_{re}(t)}$ can be obtained by the convolution between $x_{re}(t)$ and $1/\pi t$. So Eqn(2) can be rewritten as:

$$\overline{x_{re}(t)} = \frac{1}{\pi t} * x_{re}(t) \tag{3}$$

where $*$ is the convolution symbol. If Fourier transform is applied on both sides of Eqn(3), one obtains

$$\mathcal{F}\left\{\overline{x_{re}(t)}\right\} = \frac{1}{\pi} \cdot \mathcal{F}\left\{1/t\right\} \cdot \mathcal{F}\left\{x_{re}(t)\right\} = -\mathrm{j} \cdot \mathrm{sgn}(\omega) \cdot \mathcal{F}\left\{x_{re}(t)\right\} \tag{4}$$

where j is the imaginary unit; $\mathcal{F}\left\{\cdot\right\}$ denotes Fourier transform, and $\mathrm{sgn}(\cdot)$ is the sign function:

$$\mathrm{sgn}(\omega) = \begin{cases} 1 & \omega > 0 \text{ rad/s} \\ 0 & \omega = 0 \text{ rad/s} \\ -1 & \omega > 0 \text{ rad/s} \end{cases} \tag{5}$$

Using the Hilbert transform pair of $x_{re}(t)$ and $\overline{x_{re}(t)}$,the reconstructed analytic signal $x_{re}^{a}(t)$ is defined as (Oppenheim, et al. 1989):

$$x_{re}^{a}(t) = x_{re}(t) + \mathrm{j} \cdot \overline{x_{re}(t)} \tag{6}$$

Applying Fourier transform on Eqn(6), the frequency spectrum of $x_{re}^{a}(t)$ is given as

$$\mathcal{F}\left\{x_{re}^{a}(t)\right\} = \mathcal{F}\left\{x_{re}(t)\right\} + \mathcal{F}\left\{\mathrm{j}\cdot\overline{x_{re}(t)}\right\} = \left(1 + \mathrm{sgn}(\omega)\right) \cdot \mathcal{F}\left\{x_{re}(t)\right\} \tag{7}$$

As a result, $\mathcal{F}\left\{x_{re}^{a}(t)\right\} = 2\mathcal{F}\left\{x_{re}(t)\right\}$ for $\omega > 0$, $\mathcal{F}\left\{x_{re}^{a}(t)\right\} = \mathcal{F}\left\{x_{re}(t)\right\}$ for $\omega = 0$ and $\mathcal{F}\left\{x_{re}^{a}(t)\right\} = 0$ for $\omega < 0$. This means that the spectrum of the analytic signal, $x_{re}^{a}(t)$, can be easily obtained based on the calculation of $\mathcal{F}\left\{x_{re}(t)\right\}$. In addition, the time-domain expression of the analytic signal $x_{re}^{a}(t)$ can be obtained by an inverse Fourier transform to the right hand side of Eqn(7). Finally, as shown in the literature, the envelope signal of the analytic reconstructed signal $x_{re}^{env}(t)$ can be calculated as the magnitude of the analytic signal $x_{re}^{a}(t)$ (Dugundji 1958; Pertsch, et al. 2011):

$$x_{re}^{env}(t) = \left|x_{re}^{a}(t)\right| = \sqrt{x_{re}^{2}(t) + \overline{x_{re}(t)}^{2}} \tag{8}$$

4. Validation of wireless ultrasonic sensing node on a notch specimen

In order to validate the performance of the wireless ultrasonic sensing node, an experiment is first carried out on a steel specimen with four artificial notches of different depths. Then, the same ultrasonic measurement is repeated with traditional commercial equipment (an arbitrary waveform generator and an oscilloscope) to use its result as a reference. In these experiments, the wedge technique is employed to launch and detect Rayleigh waves in the steel specimen. Two commercial narrow band ultrasonic transducers (*Ultran Group*, WC50-0.5) are attached to the transmitting and receiving wedges, respectively.

Different types of ultrasonic waves, such as bulk wave, Rayleigh wave, and Lamb wave (Aindow, et al. 1981), can be used for SHM. One advantage of Rayleigh wave is that it suffers less from geometric attenuation than other bulk waves (Pertsch 2009) owing to its two-dimensional propagation nature. Moreover, Rayleigh wave is non-dispersive unlike Lamb waves, and thus, waveforms from an experiment are relatively simple and easy to analyze (Staszewski 2004). These advantages make Rayleigh wave suitable to be used for low-power ultrasonic SHM applications.

4.1. Notch specimen and measurement procedures

The specimen, which is made of steel with dimensions $241.3\ \text{mm} \times 152.4\ \text{mm} \times 25.4\ \text{mm}$, is shown in Figure 6. Four notches with different depths are cut by electrical discharge machining (EDM) as simulated cracks. The notch depths are 0.51, 1.27, 2.29, and 3.05 mm; the width is about 9.3 mm; the opening gap is about 0.58 mm long, and the distance between them is 25 mm. These notches are sufficiently away from both the specimen boundaries and each other, and thus ultrasonic measurements can be performed for each individual crack with little disturbances from boundaries and adjacent notches.

In the ultrasonic measurement, two ultrasonic transducers are placed on each side of the notch in a pitch-catch setup. The transducers are carefully aligned so that the generated waves are normally incident on and transmitted through the crack. The distance between the transducer on either side of the notch is 12.7 mm. Couplant oil is used between the wedge and the specimen surface. In the measurement taken with the wireless ultrasonic sensing node (Figure 7(a)), a 5-cycle ultrasonic tone-burst with a peak-to-peak amplitude of 18 V at 500 kHz is generated by the excitation module and fed to the transmitting transducer. The ultrasonic waves (Pertsch, et al. 2011), which are launched in the specimen, propagate through the notch and are then detected by the receiver on the other side of the notch. The received signal is amplified

as much as 30 dB and low-pass filtered with a 1 MHz cutoff frequency. The conditioned signal enters the ADC module of the *Martlet* and finally upon digitization is wirelessly sent to a computer for post-processing. Besides wireless measurement, a cabled baseline measurement is performed using the same transducer arrangement as in the previous measurements (Figure 7(b)). A same excitation signal is generated by an arbitrary waveform generator (*Agilent* 33220A) and a response signal is captured by an oscilloscope (*Tektronix* MSO4034) at the sampling frequency of 250 MHz.

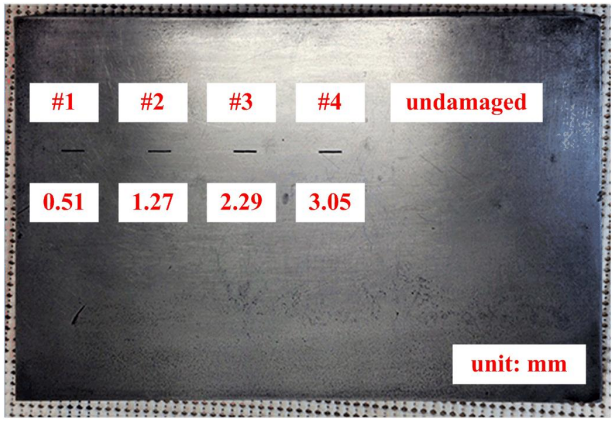

Figure 6. Steel specimen with four notches

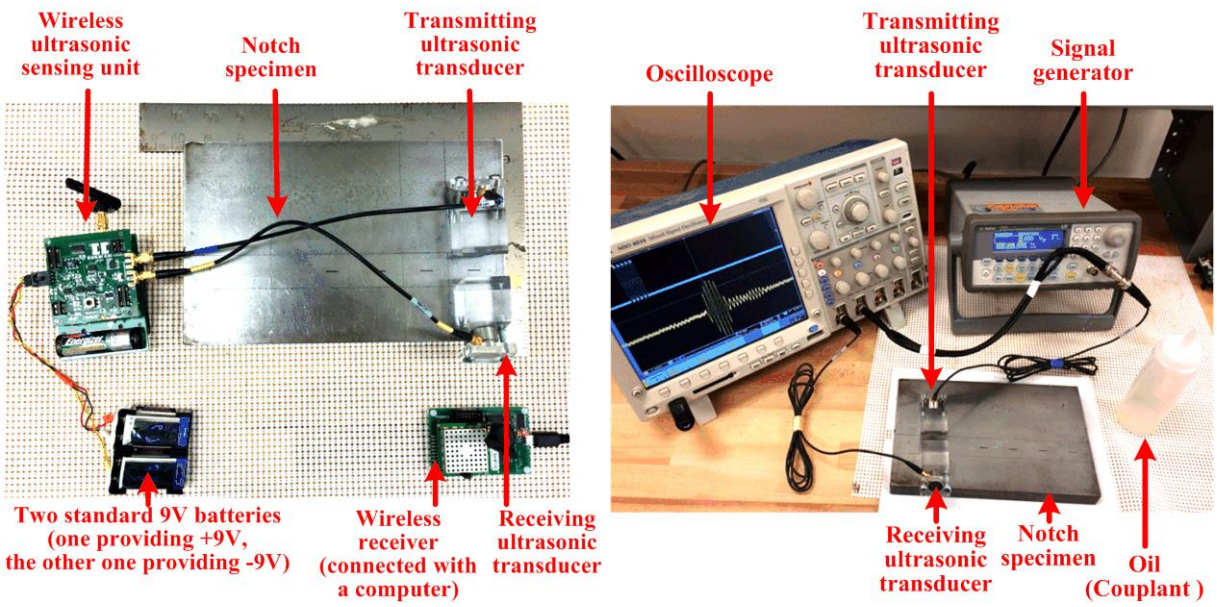

(a) Photo of the wireless test setup (b) Photo of the cabled test setup

Figure 7. Experimental setup for both cabled and wireless test

4.2. Measurement results from wireless ultrasonic sensing node and cabled equipment

The signal reconstruction algorithm is applied as described in Section 3.1, and Figure 8(a) and (b) each shows a sampled tone-burst signal (cross symbols) taken from the undamaged area and the reconstructed signal (continuous lines). Figure 8(a) shows a general scenario when peaks in the original sampled signal are missing due to the low sampling rate. In contrast, Figure 8(b) illustrates the scenario when the sampled signal coincidentally captures the peak amplitude of the original signal. The plots demonstrate that signal reconstruction helps restore the peak value of the original signal.

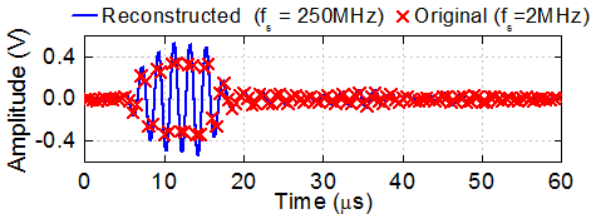

(a) Comparison between original and reconstructed wireless signals (the original missing peaks)

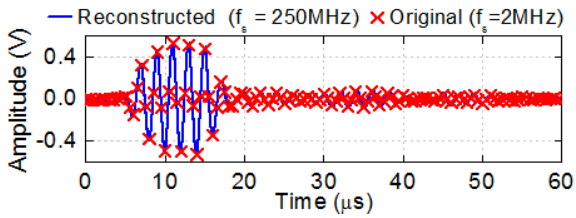

(b) Comparison between original and reconstructed wireless signals (the original including peaks)

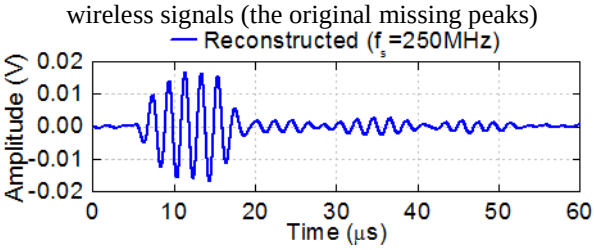

(c) Reconstructed wireless signal with gain removed

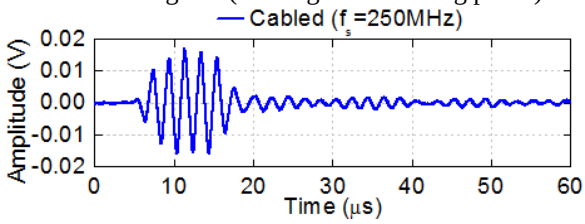

(d) Cabled signal at 250 MHz

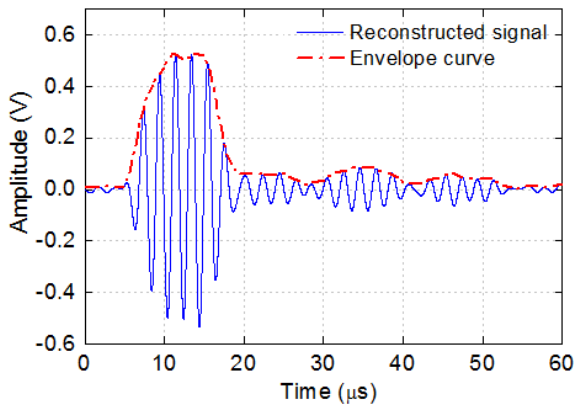

(e) Envelope of a sample tone-burst at undamaged area

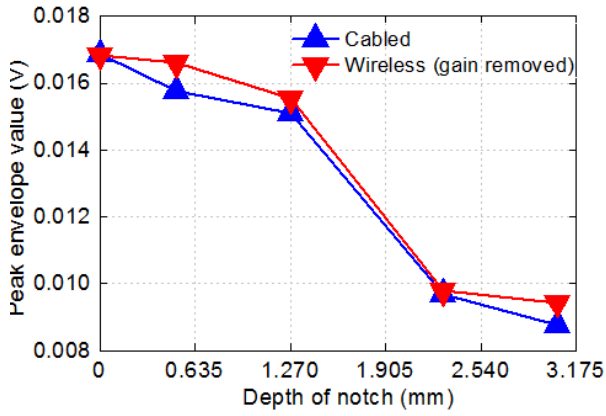

(f) Comparison of cabled and wireless peaks

Figure 8.Comparison of cabled and wireless measurement results

To validate the reconstruction performance of waveform as well, a reconstructed wireless signal (shown in Figure 8(c)) is compared with a signal captured by cabled equipment (shown in Figure 8(d)), both collected from the undamaged area. Note that a gain of 30 dB is removed from the reconstructed wireless signal so that its waveform can be compared with that of cabled signal. In order to evaluate the

waveform difference between cabled and reconstructed wireless signals, relative error (i.e. root-mean-square error, RMSE) is calculated:

$$\mathrm{RMSE} = \sqrt{\frac{1}{n}\sum_{i=1}^{n}\left(x_{cabled}\left(i\right) - x_{wireless}^{reconstructed}\left(i\right)\right)^2} \tag{9}$$

where x_{cabled} is a signal captured by cabled equipment from undamaged area at 250 MHz; $x_{wireless}^{reconstructed}$ is the corresponding reconstructed wireless signal of 250 MHz (with amplification removed for comparison). Using data plotted in Figure 8 (c) and (d), the relative error is found to be 7.53×10^{-4} V, which is small compared with the amplitude over 0.01 V. Therefore, it can be concluded that the cabled and reconstructed wireless signals are very close, and that the reconstruction algorithm can effectively rebuild the waveform. Furthermore, Figure 8(e) shows an example of reconstructed tone-burst signal together with the envelope curve extracted by DHT, as described in the Section 3.2. This particular signal has two peaks with similar magnitudes, but the envelope curve easily identifies the highest peak.

To reduce noise effect, at each notch location, average peak amplitude is obtained from the envelopes of 60 reconstructed wireless signals, and obtained from 15 cabled signals. The results are compared in Figure 8(f). This figure shows that the average peak amplitudes of the signals taken from the wireless and cabled equipment are in good agreement. There is a clear trend that the peak amplitude of the transmitted signals decreases with the increasing of the notch depth. This is because more energy of the incident Rayleigh wave is scattered and reflected from a deeper notch and thus less energy is captured by the receiving transducer on the other side.

These results illustrate that the *Martlet* wireless ultrasonic sensing node is capable of generating, detecting, and post-processing signals in 500 kHz range in the experiment where ultrasonic signals propagate through a notch of a few millimeters depth. Moreover, the resulting signals, after the signal reconstruction and envelope detection, are almost equivalent to those of cabled ultrasonic experiment. Finally, the detected signals are sensitive to the surface defects in the steel specimen and thus can be used to distinguish the notch (or crack) depth.

5. Fatigue crack monitoring using the wireless ultrasonic sensing device

In order to evaluate the possible crack detection capability of the wireless ultrasonic sensing device in a more realistic fatigue scenario, the device is applied, in-situ, to a specimen undergoing fatigue test. In this

experiment, a dog-bone specimen is cut from a 6.35 mm thick Aluminum 6061-T6-alloy plate. To facilitate fatigue crack initiation at the desired location, i.e. in the middle of the specimen, a through-thickness hole with a diameter of 3.81 mm is drilled in the middle and then two small slots are cut on both lateral sides of the hole. The detailed dimensions of the dog-bone specimen are shown in Figure 9(a). The hatched areas ($6.35\ \text{mm} \times 31.75\ \text{mm}$) in this figure indicate the locations, where two ultrasonic transducers are placed. The specimen is then fatigued under a constant-amplitude loading condition.

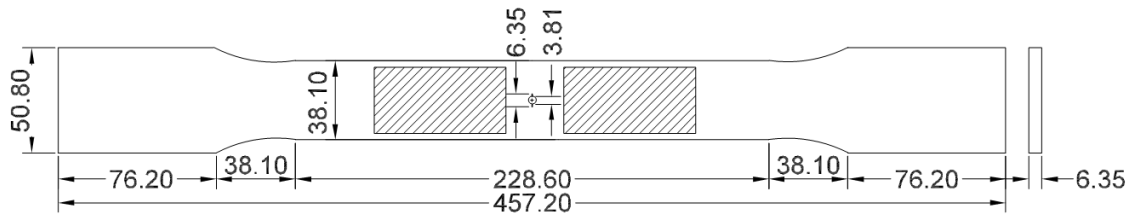

(a) Detailed dimensions of the dog-bone specimen for fatigue test (unit: mm)

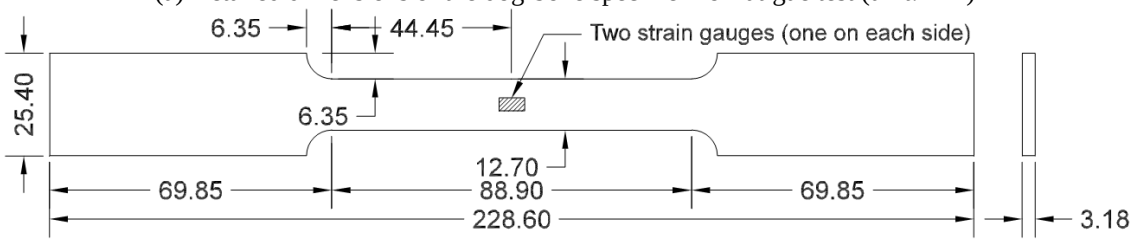

(b) Layout of flat plate tension specimen for yield strength test (unit: mm)

Figure 9. Details in the specimens' design

5.1. Material properties determination

A prior knowledge of the actual yield strength of the specimen is critical to determine fatigue-loading parameters. Thus, a tensile test is carried out on an *Instron* 22EMF material test machine with a maximum loading capacity of 245 kN. The flat plate tension test specimen is designed according to the ASTM standard E8/E8M-13a (ASTM 2013) as shown in Figure 9(b). Two 120 Ω strain gauges are attached onto both sides of the specimen and the strain data are collected with a data acquisition module (*National Instruments*, 9235) as shown in Figure 10(a). The tensile loading schedule is designed according to the above standard as well; the loading rate is set as 0.13 kN/s. The test result is shown in Figure 10(b). The yield strength determined from the curve is 294 MPa, and Young's modulus is 65.3 GPa.

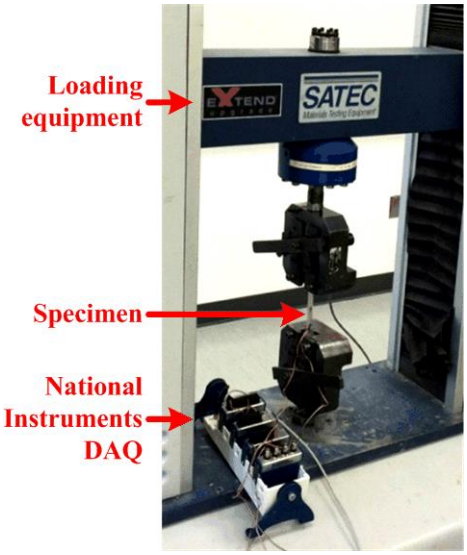

(a) Layout of the tensile test

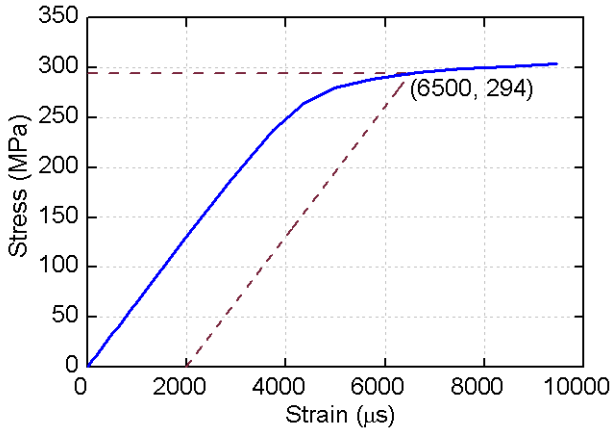

(b) Strain-stress curve for aluminum 6061-T6 under uniaxial load (average strain)

Figure 10. Test to determine Aluminum 6061-T6 yield strength

5.2. Fatigue load and test procedure

The loading parameters for fatigue test are determined according to both the ASTM standard E647-13 (ASTM 2013) and the yield strength result of the Aluminum 6061-T6material. In a preliminary fatigue test, the maximum and minimum loads are 26.69 kN and 0 kN with the R factor equaling to 0 ($R = P_{\min} / P_{\max}$). However, due to the limitation of the loading machine, the minimum load cannot be controlled to be precisely at 0 kN, and thus, is set to be a small value at 0.44 kN. The final loading profile is presented in Figure 11(a), and other detailed loading parameters are shown in Table.1. The static loading steps are allocated for collecting ultrasonic signals when the specimen is held at a static load. Different holding loads may cause different levels of crack opening.

The setup of the test is shown in Figure 11(b). At the beginning of the test, the specimen is pre-fatigued to generate an initial crack (in fact, cracks happen on both sides of the central hole), whose length is measured using a caliper. The transducers are attached to the front side of the specimen with oil couplant. The ultrasonic response signals are collected at each static holding load. Sampling frequency for wireless acquisition is 2 MHz. In addition, the received signals are post-amplified by 30 dB.

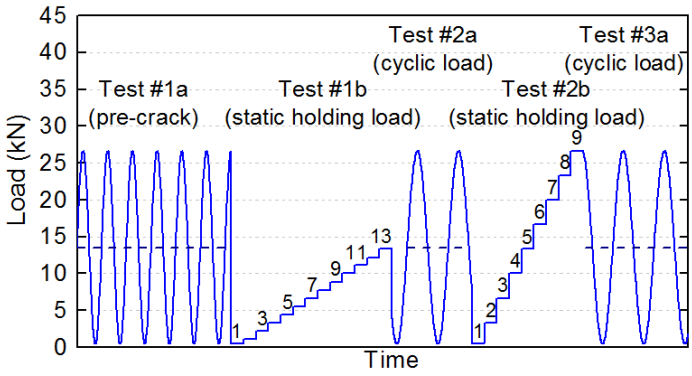

(a) Diagram of load profile to monitor crack initiation and evolution (showing up to Test #3a for brevity)

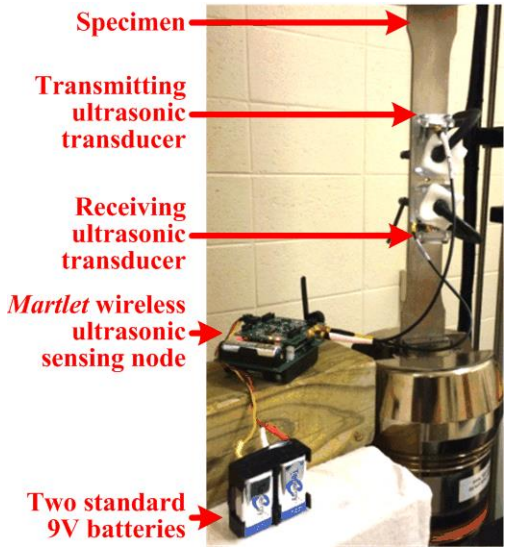

(b) Photo of the fatigue test with the wireless ultrasonic devise implemented

Figure 11. Loading parameters and experimental setup of the fatigue test

Table.1. Fatigue test loading procedures

Test No.	Test type	Loading description
#1a (Pre-crack)	Cyclic load	0.44~26.69 kN at 5 Hz; 2,000 cycles
#1b (after #1a)	Static holding load	13 steps at 0.44~13.34 kN; load increment from 1st to 2nd holding step is 0.67 kN, and 1.11 kN for steps afterwards
#2a	Cyclic load	0.44~26.69 kN at 3 Hz; 1,000 cycles
#2b (after #2a)	Static holding load	9 steps at 0.44~26.69 kN; load increment from 1st to 2nd holding step is 2.9 kN, and 3.34 kN for steps afterwards
#3a	Cyclic load	same as Test#2a
#3b (after #3a)	Static holding load	same as Test #2b
#4a	Cyclic load	same as Test #2a
#4b (after #4a)	Static holding load	same as Test #2b

5.3. Crack behavior and ultrasonic signal versus loading cycles

The crack lengths are measured throughout the fatigue test and after the specimen's failure at 5,873 cycles (on the fracture surfaces). Figure 12(a) presents the measurement results, where stable crack propagation is observed. The crack growth rate is approximately 7.62×10^{-4} mm/cycle at the beginning and sharply increases to 1.4×10^{-2} mm/cycle at the end. Since the fatigue crack growth rate has a positive correlation with the mechanical driving force for crack propagation (Jogi, et al. 2008), the fatigue crack growth rate can indicate the crack stage in the fatigue test (Logsdon and Liaw 1986). In the beginning of

the test, a plane-strain condition predominates. However, loss of constraint is expected, as the crack grows longer than a critical length, and the initial steady fatigue crack propagation mode switches to a fast fracture mode. The fractography result (Figure 12(b)) also agrees with this explanation as a clear flat-to-slant transition is observed on both sides of the fracture surface. Since during the crack propagation period, the crack growth is stable and slow enough, the presented ultrasonic method is suitable for detecting the development of small fatigue cracks.

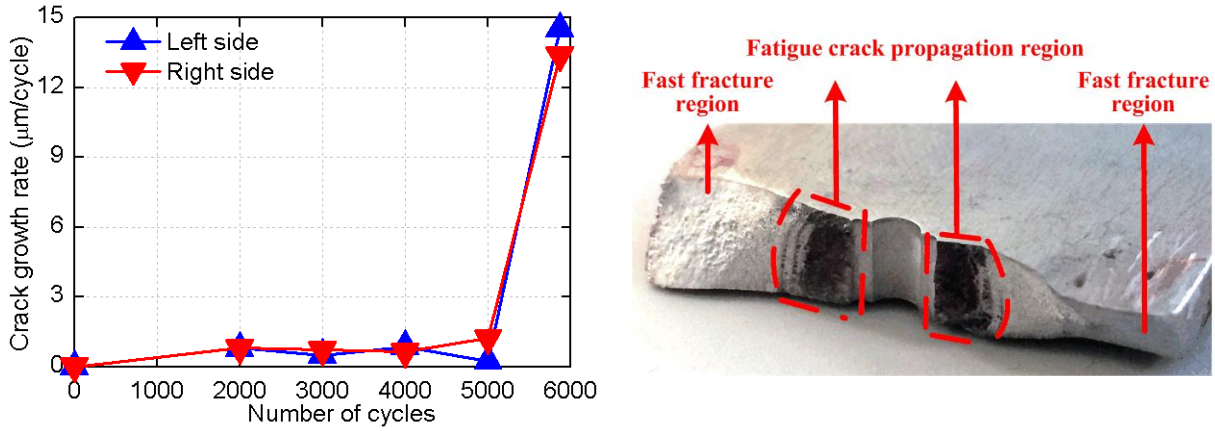

(a) Crack growth rate against loading cycles (b) Fractography result at the fracture surface

Figure 12. Growth behavior and fractography result of the crack

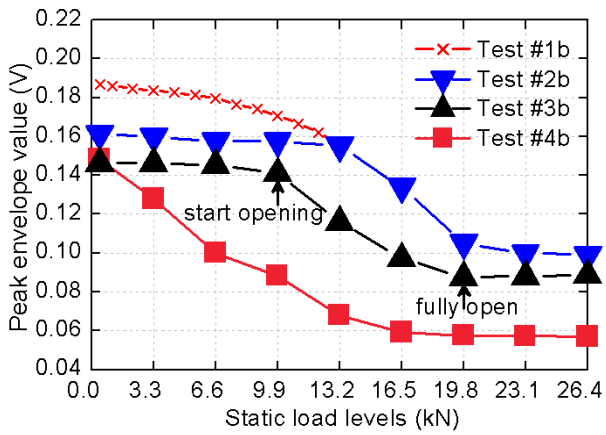

Figure 13. Average amplitude of the envelope curves of ultrasonic receiving signals at every holding load stage

At every static holding step, the ultrasonic signals are captured by the wireless ultrasonic sensing node and wirelessly transmitted. The ultrasonic data are processed by the algorithms described in Section 4.2. The peak amplitudes of the transmitted wave signals obtained from envelopes are plotted in Figure 13. In this figure, it is seen that the amplitude decreases significantly with the increase of the load at which the ultrasonic signal is taken. This trend is in good agreement with previous literature (Hevin, et al. 1998). This

can be attributed to the fact that more energy is reflected and thus less energy is transmitted and detected by the receiving transducer as the length of the cracks growing. Since the amplitude of a received ultrasonic signal correlates directly with the crack length, the change in the ultrasonic amplitude can be used to detect crack growth.

Another trend that can be observed in Figure 13 is the decreasing signal amplitude with the increase of static holding load level. This is due to the phenomenon called crack closure, which is well recognized in the fatigue-fracture community (Elbert 1971) and from the ultrasonic response from a closed crack (Rokhlin and Kim 2003). When the specimen is unloaded, small fatigue cracks initiated in ductile metals (e.g. Aluminum 6061-T6) tend to close, for reasons including the closing action of the crack tip plasticity. At low holding load levels, the tensile load is not high enough to open the cracks (see the beginning parts of Test #1b, #2b, and #3b in Figure 13), so the crack surfaces are still tightly closed and thus allow the surface Rayleigh wave to transmit through. This has led to the stable ultrasonic signal amplitudes, i.e. the plateau region in the beginning parts of Test #1b, #2b, and #3b in Figure 13. As the holding load level increases further and the cracks open gradually, the amplitude of the transmitted ultrasonic signals starts to decrease with load. After the load gets to some higher load, and the crack fully opens, the amplitude of the transmitted ultrasonic signal saturates at a lower holding load level. This opening-closure behavior is well illustrated in the ultrasonic signals, especially the signals collected in Test #3b, where the arrows indicate the start and end of the opening.

A very similar behavior is observed in the reflected ultrasonic signals from a surface crack initiated around a surface defect. However, this trend is different near the end of the fatigue life (i.e. at 5,000 cycles), and the initial flat stage is missing in the curve. This phenomenon is attributed to the stress release. When the specimen is on the brink of failure, the stress required to open a crack decreases significantly (Rokhlin and Kim 2003). As demonstrated at the beginning part of Test #4b in Figure 13, it is possible that the stress for the crack to open is so small that the plateau region would not appear. The same phenomenon has also been described and reported in other investigations (Kim and Rokhlin 2002; Song and Sih 2003). At a given number of fatigue cycles, the crack length designates the length of the fully open crack. Therefore, if the holding load level is not carefully taken into consideration, the ultrasonically determined crack length can be significantly underestimated. More detailed quantitative analysis is required in subsequent studies.

6. Conclusions and discussions

This paper presents the design and validation tests of a wireless ultrasonic sensing node, which is developed based on the *Martlet* platform for wireless sensing.

(1) Powered by two standard 9V batteries, the ultrasonic wing can generate ±9 V PWM signals at 500 kHz for ultrasonic excitation. Meanwhile, the device performs signal conditioning to receive ultrasonic signal for a higher signal-to-noise ratio. The conditioned signal can be sampled at up to megahertz-level by the *Martlet* sensing node, and then wirelessly transmitted.

(2) So as to obtain a more accurate assessment of the peak amplitude of the received ultrasonic signal, a two-step data processing approach is introduced (i.e. signal reconstruction and envelope identification using discrete Hilbert transform). Furthermore, experimental results show the proposed approach is effective for accurately capturing signal peaks.

(3) Validation test for the wireless ultrasonic sensing node is carried out using a notch specimen, in order to evaluate the performance of surface defect detection. Experimental results demonstrate that the wireless ultrasonic sensor signal is sensitive to surface defects, and is reasonably close to that of a cabled NDT system.

(4) Performance of the wireless ultrasonic sensing node is further validated through fatigue test of a dog-bone specimen. The experimental results show agreement with those in previous studies, and can be explained by crack scattering theory. The reliability of the wireless ultrasonic sensing node is validated.

This study is undertaken as a first step toward the development and testing of the ultrasonic functionality with the *Martlet* wireless sensing platform. Future efforts are needed towards more detailed and quantitative evaluation of damage. The study will become more interesting if the ultrasonic measurements can be used to predict the fatigue life of a structural member. Furthermore, upon successful laboratory validation, field deployment of the miniature wireless devices will be the next step towards enabling unprecedentedly dense and long-term ultrasonic measurements for critical structural members in the field.

7. Acknowledgements

This research is partially sponsored by the National Science Foundation (#CMMI-1150700), the Research and Innovative Technology Administration of US DOT (#DTRT12GUTC12), and the Georgia

DOT (#RP12-21). The authors also wish to express their gratitude to Dapeng Zhu, Xiaohua Yi and Andrew Udell of Georgia Institute of Technology for their assistance during the design and testing of the *Martlet* ultrasonic wing. Any opinions, findings, and conclusions or recommendations expressed in this publication are those of the authors and do not necessarily reflect the view of the sponsors.

References

Aindow A, Dewhurst R, Hutchins D, et al. (1981). "*Laser-generated ultrasonic pulses at free metal surfaces*", The Journal of the Acoustical Society of America, Vol. 69, No. 2, pp. 449-455.

ASTM E647-13 (2013). *Standard test method for measurement of fatigue crack growth rates*, ASTM, USA.

ASTM E8/E8M-13a (2013). *Standard test methods for tension testing of metallic materials*, ASTM, USA.

Baker J, Hasler W L, Camilleri M, et al. (2011). "*Impairment of overall and regional high amplitude colon contractions in severe slow transit constipation measured by wireless motility capsules*", Gastroenterology, Vol. 140, No. 5, pp. S-531.

Cooklev T (2004). *Wireless Communication Standards: a Study of IEEE 802.11, 802.15, and 802.16*. USA, Standards Information Network IEEE Press.

Dhakal D R, Neupane K, Thapa C, et al. (2013). "*Different techniques of structural health monitoring*", Research and Development (IJCSEIERD), Vol. 3, No. 2, pp. 55-66.

Dong X, Chen S, Zhu D, et al. (2014). *High-speed heterogeneous data acquisition using Martlet-A next-generation wireless sensing node*, 6th World Conference on Structural Control and Monitoring, Rarcelona.

Dugundji J (1958). "*Envelopes and pre-envelopes of real waveforms*", Information Theory, IRE Transactions on, Vol. 4, No. 1, pp. 53-57.

Elbert W (1971). *The significance of fatigue crack closure*. Damage Tolerance in Aircraft Structures, STP 486. USA, American Society for Testing and Materials: 230-242.

Grosse C, Finck R, Kurz J, et al. (2004). *Monitoring techniques based on wireless AE sensors for large structures in civil engineering*, 26th European Conference on Acoustic Emission Testing, Berlin, Germany.

Hevin G, Abraham O, Pedersen H, et al. (1998). "*Characterization of surface cracks with Rayleigh waves: a numerical model*", NDT & E International, Vol. 31, No. 4, pp. 289-297.

Huang N E, Shen Z, Long S R, et al. (1998). "*The empirical mode decomposition and the Hilbert spectrum for nonlinear and non-stationary time series analysis*", Proceedings of the Royal Society of London. Series A: Mathematical, Physical and Engineering Sciences, Vol. 454, No. 1971, pp. 903-995.

Jogi B, Brahmankar P, Nanda V, et al. (2008). "*Some studies on fatigue crack growth rate of aluminum alloy 6061*", Journal of materials processing technology, Vol. 201, No. 1, pp. 380-384.

Kane M, Zhu D, Hirose M, et al. (2014). *Development of an extensible dual-core wireless sensing node for cyber-physical systems*, Sensors and Smart Structures Technologies for Civil, Mechanical, and Aerospace Systems, San Diego.

Kim J-Y and Rokhlin S I (2002). "*Surface acoustic wave measurements of small fatigue cracks initiated from a surface cavity*", International journal of solids and structures, Vol. 39, No. 6, pp. 1487-1504.

Logsdon W and Liaw P K (1986). "*Tensile, fracture toughness and fatigue crack growth rate properties of silicon carbide whisker and particulate reinforced aluminum metal matrix composites*", Engineering Fracture Mechanics, Vol. 24, No. 5, pp. 737-751.

Lynch J P and Loh K J (2006). "*A summary review of wireless sensors and sensor networks for structural health monitoring*", Shock and Vibration Digest, Vol. 38, No. 2, pp. 91-130.

Lynch J P, Wang Y, Loh K J, et al. (2006). "*Performance monitoring of the Geumdang Bridge using a dense network of high-resolution wireless sensors*", Smart Materials and Structures, Vol. 15, No. 6, pp. 1561.

Monje P M, Casado L, Aranguren G, et al. (2012). *Integrated electronic system for ultrasonic structural health monitoring*, 6th European Workshop on Structural Health Monitoring, Dresden, Germany.

Nakamura I, Saeki M, Oguni K, et al. (2013). "*Energy-Saving Wireless Sensor Node for Relative Positioning of Densely Deployed GPS Network*", Journal of Infrastructure Systems, Vol. 20, No. 2, pp. 04014003-1-10.

Nyquist H (1928). "*Certain topics in telegraph transmission theory*", Transactions of the American Institute of Electrical Engineers, Vol. 47, No. 2, pp. 617-644.

Ohtsu M (1996). "*The history and development of acoustic emission in concrete engineering*", Magazine of concrete research, Vol. 48, No. 177, pp. 321-330.

Oppenheim A V, Schafer R W and Buck J R (1989). *Discrete-time signal processing*. Upper Saddle River, USA, Prentice-Hall Inc.

Pertsch A (2009). *An intelligent stand-alone ultrasonic device for monitoring local damage growth in civil structures*, PhD Thesis, Georgia Institute of Technology, Atlanta.

Pertsch A, Kim J Y, Wang Y, et al. (2011). "*An intelligent stand-alone ultrasonic device for monitoring local structural damage: implementation and preliminary experiments*", Smart Materials and Structures, Vol. 20, No. 1, pp. 015022.

Rokhlin S I and Kim J-Y (2003). "*In situ ultrasonic measurement of crack closure*", International journal of fatigue, Vol. 25, No. 1, pp. 51-58.

Shannon C E (1948). "*A mathematical theory of communication*", Bell Systems Tech, Vol. 27, No. pp. 379-423.

Shannon C E (1949). "*Communication in the presence of noise*", Proceedings of the IRE, Vol. 37, No. 1, pp. 10-21.

Song Z and Sih G (2003). "*Crack initiation behavior in magnetoelectroelastic composite under in-plane deformation*", Theoretical and Applied Fracture Mechanics, Vol. 39, No. 3, pp. 189-207.

Staszewski W J (2004). *Structural health monitoring using guided ultrasonic waves*. Advances in Smart Technologies in Structural Engineering. J. Holnicki-Szulc and C. Soares. Germany, Springer Berlin Heidelberg. 1: 117-162.

Viktorov I A (1967). *Rayleigh and Lamb waves: physical theory and applications*. New York, Plenum Press.

Warneke B A and Pister K S (2004). *An ultra-low energy microcontroller for smart dust wireless sensor networks*, IEEE International Solid-State Circuits Conference, San Francisco, USA.

Yaroslavsky L (2007). *Fast discrete sinc-interpolation: a gold standard for image resampling*. Advances in Signal Transforms: Theory and Applications. Egypt, Hindawi Publishing Corporation.

Zhu D, Wang Y and Brownjohn J (2011). "*Vibration testing of a steel girder bridge using cabled and wireless sensors*", Frontiers of Architecture and Civil Engineering in China, Vol. 5, No. 3, pp. 249-258.